Available online at www.sciencedirect.com
SCIENCE DIRECT®
Vision Research 44 (2004) 1065–1077
Vision Research
www.elsevier.com/locate/visres

The influence of motion-defined form on the perception of spatially-defined form

Stéphane J.M. Rainville *, Hugh R. Wilson

Center for Vision Research, York University, 4700 Keele Street, North York, Ont., Canada M1J 1P3

Received 11 June 2003; received in revised form 28 November 2003

Abstract

It is well established that the visual system is sensitive to the global structure—or "form"—of objects defined exclusively by spatial or motion cues, but it remains unclear how form perception combines spatial and motion cues if these are presented concurrently. In the present study, we introduce a novel class of stimuli where spatial-form and motion-form can be superimposed and manipulated independently. In both the spatial and motion domains, global structure consisted of radial-frequency (RF) contours defined by a virtual circle of Gabor elements whose positions and/or drift speeds were sinusoidally modulated at a specified frequency of polar angle. The first two experiments revealed that observers encode the global structure of spatial-RF and motion-RF contours presented in isolation. In a third experiment, observers detected a spatial-RF modulation superimposed on a motion-RF pedestal of identical radial frequency: results showed little facilitation at low pedestal amplitudes but significant masking at higher pedestal amplitudes, especially if the RF modulations of test and pedestal were in anti-phase. Additional experiments demonstrated that masking of the spatial-RF test is abolished if the global structure of the motion-RF pedestal is altered or destroyed while local motion cues are preserved. We argue these results cannot be explained by local neural interactions between spatial and motion cues and propose instead that data reflect higher-level interactions between separate visual pathways encoding spatial-form and motion-form.

Keywords: Spatial; Motion; Form; Local; Global; Interaction; Radial frequency; Feedback

1. Introduction

Human vision has evolved to recover key information from the environment. Because ecologically meaningful information resides at the level of objects and their interrelationships in the natural world, there is a survival premium on encoding their global structure—or "form". However, the initial stages of human vision are mediated by local mechanisms akin to filters that integrate information over restricted portions of the visual field (DeAngelis, Freeman, & Ohzawa, 1994; Hubel & Wiesel, 1968). These filters are selective for image features such as spatial scale (Campbell & Robson, 1968; De Valois & Tootell, 1983), orientation (Blakemore & Campbell, 1969; Hubel & Wiesel, 1968), temporal scale (Fredericksen & Hess, 1997; Lehky, 1985; Mandler & Makous, 1984; Pinter & Harris, 1981) and motion (Anderson & Burr, 1987; Hubel & Wiesel, 1968), but their limited spatial extent essentially makes these filters blind to the global arrangement of local image features. How later visual stages combine local information into a representation of global structure remains one of the fundamental problems currently tackled by vision science.

Psychophysical evidence demonstrates that human observers can pool information from local mechanisms to extract form information defined either by spatial cues or motion cues alone. An instance of spatial-form perception is the detection of a string of collinear texture elements embedded in a sea of randomly oriented elements (Field, Hayes, & Hess, 1993) as this analysis is mediated by linking the outputs from local mechanisms (Hess & Dakin, 1997). Similarly, observers can recover instances of motion-form (often refered to as "structure-from-motion") such as rotation, expansion, or biological motion which can only be detected via a non-local analysis (Bex & Dakin, 2002; Loffler & Wilson, 2001; Lorenceau, 1996; Lorenceau & Shiffrar, 1992;

* Corresponding author. Tel.: +1-416-7362100x33325; fax: +1-416-7365857.
E-mail address: rainvill@yorku.ca (S.J.M. Rainville).

0042-6989/$ - see front matter © 2004 Elsevier Ltd. All rights reserved.
doi:10.1016/j.visres.2004.01.003

Mingolla, Todd, & Norman, 1992; Morrone, Burr, & Vaina, 1995; Verghese & Stone, 1995). However, while the visual pathways sensitive to spatial-form and motion-form have been studied extensively (Goodale & Milner, 1992; Merigan & Maunsell, 1993; Wilson, 1999; Wilson, Ferrera, & Yo, 1992), the nature of cross-pathway interactions remains less understood.

Accumulating evidence suggests that spatial cues influence the perception of motion-defined form (Alais, van der Smagt, van den Berg, & van de Grind, 1998; Croner & Albright, 1997; Geisler, 1999; Li & Kingdom, 1999, 2001; Ross, Badcock, & Hayes, 2000). In particular, the perception of motion-form is reportedly inhibited—or "vetoed"—if spatial cues are inconsistent with collinear (Lorenceau & Zago, 1999) or closed-contour arrangements (Lorenceau & Alais, 2001). However, only a handful of studies have investigated the opposite condition, namely the influence of motion cues on the perception of form defined by spatial cues (i.e. spatial-form). This small number of studies presumably reflects the fact that it is difficult to construct stimuli where spatial-form is preserved in displays where local spatial and motion cues are superimposed.

In one study that tested the effect of motion cues on spatial-form perception, observers detected a path of drifting collinear Gabor elements embedded in a sea of drifting distractor elements with random orientations (Hayes, 2000). In the key condition, the spatial position of each Gabor element composing the path was physically offset in one of two randomly-chosen directions perpendicular to the path's backbone. Although such random positional offsets impair path detection in static displays, path detection improved if Gabor elements drifted towards the path's backbone, as if the motion of each element counteracted its spatial offset; by comparison, path detection deteriorated further if Gabors drifted in a direction away from the path's backbone. The author interpreted these findings as evidence that local motion cues can masquerade as spatial cues in contour integration and that mechanisms mediating contour detection encode the *perceived* rather than the *physical* position of local features.

In a study that revisited path detection with drifting Gabors (Bex, Simmers, & Dakin, 2001), observers were shown stimuli in which path elements drifted in the same direction relative to the path's backbone but where the drift speed of each element from the display (whether a member of the path or of the distracter set) was randomly selected from a range of speeds covering several octaves. Results revealed that paths composed of a heterogeneous ensemble of drift speeds were detected as easily as paths composed of homogeneous speeds and that path detection with drifting Gabors is easier than in purely static displays. The authors concluded that mechanisms encoding spatial contour information receive an input from the motion system but are broadly tuned for temporal frequency.

The studies reviewed in the previous two paragraphs were essentially concerned with how spatial-form perception is affected by *local motion* rather than by *motion-form*: indeed, both types of stimuli generally lacked motion-form because, in most conditions, either the direction or the speed of the drift was independently and randomly determined for each Gabor. In the present paper, we ask the question: How does motion-form influence the perception of spatial-form? Answering this question requires stimuli where motion-form and spatial-form can coexist without *physically* interferring with each other. The stimuli used in the experiments reported here meet those constraints and consist of radial-frequency (RF) contours defined either in the spatial domain, the motion domain, or both. Results showed that observers encode the global structure of spatial-form and motion-form when each is presented in isolation, but that motion-form pedestals can selectively mask spatial-form perception when both form types are presented concurrently. Additional experiments revealed that motion-form, not local motion cues per se, interferes with spatial-form perception and point to higher-level interaction between separate mechanisms encoding spatial-form and motion-form.

2. Method

2.1. Observers

The first author (SR) and five naive observers (AC, CH, DG, DR, and MK) participated in the study. All observers had normal or corrected-to-normal vision.

2.2. Hardware and calibration

Experiments were carried out on an iMac hosting a standard 8-bit/gun color video card driving a built-in 15-in. CRT monitor with a linearized grayscale look-up table with 151 entries. Spatial resolution was set to 640×480 pixels and the display was run at a refresh rate of 120 Hz although each stimulus frame was presented for two refreshes, or an effective frame rate of approximately 60 Hz. After calibration, the display had a mean luminance of 46.0 cd/m^2. Stimuli were generated in the Matlab 5.2.1 environment and displayed using software from the Psychophysics Toolbox (Brainard, 1997) calling lower-level routines from the VideoToolbox (Pelli, 1997).

2.3. Stimuli

Fig. 1 illustrates stimuli composed of 36 Gabor elements forming radial-frequency (RF) contours. The

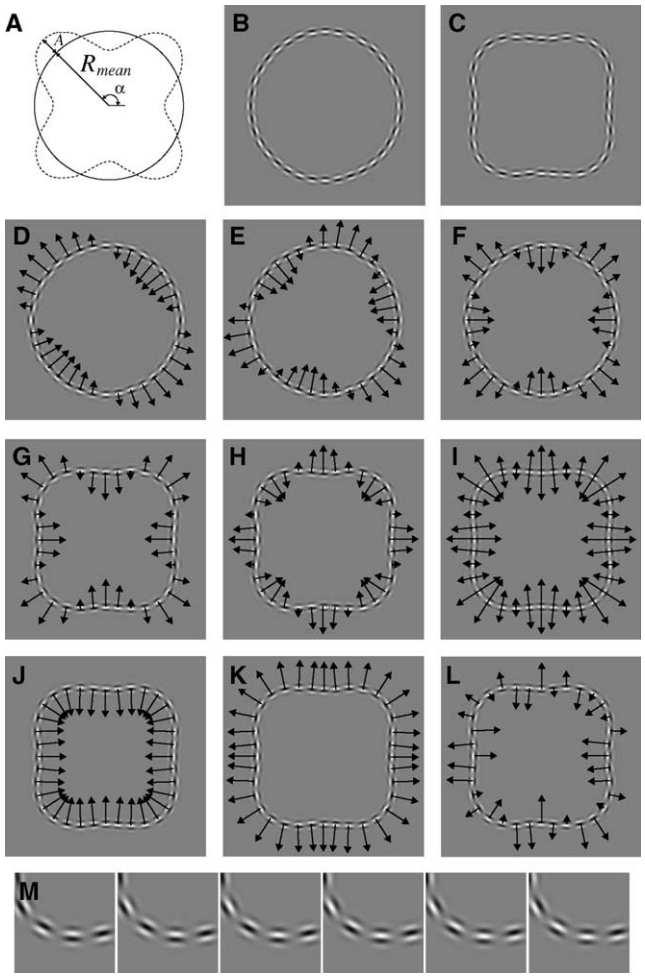

Fig. 1. Spatially-defined and motion-defined RF stimuli. (A) Geometry of an RF4 stimulus: a closed circular contour is sinusoidally modulated as a function of polar angle. The RF4 contour has a mean radius R_{mean} and contains four cycles of a sinusoidal modulation with amplitude A. (B, C) Pure spatial-RF4 contours with modulation amplitudes of 0.0 and 0.15 respectively. Contours are sampled by Gabor elements with random carrier phases. (D–F) Pure motion-RFs with 2, 3, and 4 cycles. Arrows indicate the speed and direction of gratings drifting behind static Gaussian apertures. (G–L) Various motion pedestals superimposed on a spatial-RF4 test. (G and H) Motion-RF4 pedestals either in-phase or in anti-phase with the test. (I) Flickering (i.e. counterphasing) pedestal obtained from the combination of in-phase and anti-phase motion-RF4 pedestals as indicated by the bi-directional arrows. (J and K) Motion-RF0 pedestals with either negative (i.e. contraction) or positive (i.e. expansion) modulation amplitudes. (L) Motion-RF4 pedestals whose local speeds have been randomly permuted between Gabor elements. (M) Zoom on six successive frames of a motion-RF4 pedestal in phase with a spatial-RF4 test (similar to panel G). Note that the outline of the contour (defined by Gabor position and orientation) remains static as gratings drift at different speeds.

geometry of an RF contour is best described in polar coordinates (illustrated in panel A) as a closed contour whose radius varies sinusoidally as a function of polar angle α. The term radial frequency corresponds to the number of sinusoidal cycles for one full rotation around the clock face (360°), and this value is necessarily an integer to prevent wrap-around discontinuities. The general equation for an RF contour R is

$$R = R_{\text{mean}}[1 + A \cdot \cos(\omega\alpha + \beta)] \quad (1)$$

where R_{mean} is the radius of the circle, A is the amplitude of the sinusoidal modulation, ω is radial frequency, and β determines the phase of the modulation—or, equivalently, the orientation of the RF modulation in the xy plane. The RF's modulation amplitude A is constrained not to exceed 1.0. Panels B and C of Fig. 1 show spatial RF contours with modulation amplitudes of 0.0 and 0.15.

For spatially bandpass RF contours, human thresholds for discriminating between a perfect circle and a radially modulated version fall in the hyperacuity range and correspond to modulation amplitudes in the order of 0.4% of the pattern's mean radius (Wilkinson, Wilson, & Habak, 1998). These amplitude thresholds are considerably lower than those for the probabilistic pooling of local curvature estimates and strongly suggest that radial frequency detection involves mechanisms sensitive to global spatial structure which extract object information by actively integrating across local stimulus features (Loffler, Wilson, & Wilkinson, 2003; Wilkinson et al., 1998).

The obvious counterpart to a spatial-RF contour in the motion domain is a motion-RF contour in which the *speed* assigned to local elements is a sinusoidal function of polar angle. As with spatial-RFs, motion-RFs have a radial frequency, a modulation amplitude that defines the speed of each element, and a modulation phase that specifies how the motion-RF is oriented in the xy plane. Note that, throughout the present paper, motion-RFs do not contain the "dc" radius component that is necessary to define the absolute size of the contours in space. Examples of motion-RFs with radial frequencies of 2, 3, and 4 cycles are shown in panels D through F of Fig. 1.

Fig. 1 also shows several examples of stimuli where a spatial-RF4 contour is superimposed on various motion pedestals (panels G through L). In some of these examples, the speed of individual elements is consistent with global motion-defined form; for instance, in panels G and H, a motion-RF4 is either in-phase or in anti-phase with respect to the spatial-RF4 test. The specific properties of each panel are described in the figure caption and in relevant sections of the paper. Panels in M show a close-up view of six successive frames in which the spatial-RF4 test and the motion-RF4 pedestal are in phase; the purpose here is to illustrate that while Gabors drift at different (but constant) speeds, the orientation and position of each element remains the same, and therefore the spatial information that defines the test stimulus is unaffected by the superimposed motion pedestal.

Throughout all experiments, Gabors had a carrier spatial frequency of 7.8 cpd (wavelength of 8 pixels) and a Gaussian space constant of 3.85 min of arc (4 pixels). RF contours had a mean radius of 1.6° of visual angle (100 pixels), were scaled to 100% Michelson contrast, and were presented for a total of for 29 frames (or approximately 483 ms at 60 Hz). At a maximum motion amplitude of 1.0, the fastest-moving elements underwent 90° phase jumps between frames (i.e. the quarter-cycle limit) for a drift speed of 1.92°/s. To minimize transients, the contrast of the display was ramped between 0% and 100% using a Gaussian temporal window with a time constant of 62.5 ms. Additional mathematical specifications for the stimuli can be found in Appendix A.

2.4. Procedure

Viewing distance was set to 160 cm such that one pixel subtended 1.0 min of arc. In all experiments but Experiment 2, observers discriminated between a spatial-RF test and a zero-amplitude (i.e. a circle) comparison (see panels B and C of Fig. 1) in a two-alternative forced-choice (2AFC) paradigm that used a method of constant stimuli. The order of presentations was randomly interleaved across trials, and observers pressed one of two keys to report the interval that contained the spatial-RF modulation and guessed if necessary. Stimulus presentations were separated by a minimum inter-trial interval of 250 ms, and no auditory feedback was provided.

Data were collected for several modulation amplitudes that were randomly chosen across trials. While the total number of amplitude levels and trials varied across conditions and observers, no fewer than 100 trials were included in the computation of every data point. We fitted two-parameter cumulative normals to the percent-correct vs. modulation-amplitude data using a maximum-likelihood criterion and estimated thresholds at the 75%-correct performance level. Error bars showing 95% confidence intervals (±2 SD) were computed using a bootstrapping technique (Efron & Tibshirani, 1993) that modeled our data as a binomial random process. We computed 250 samples from this process, fitted a cumulative normal to each sample, and obtained a distribution of threshold values whose standard deviation we used to compute confidence intervals.

3. Detecting spatial RFs

The purpose of the first experiment was to obtain baseline detection thresholds for spatial-RF contours sampled by Gabors. We measured detection amplitude thresholds for RFs of 2, 3, and 4 cycles for each of two conditions. In the first condition, all Gabor elements were in cosine phase whereas in the second condition phases were independently randomized. The random-phase condition provides a better baseline against which thresholds involving superimposed motion masks can be benchmarked since the phases of elements moving at different speeds necessarily become offset even if initial phases are identical.

Fig. 2 shows results for three observers (DG, DR, and SR) where spatial-RF amplitude thresholds (expressed as a proportion of mean radius, or Weber fraction) are plotted as a function of radial frequency. As for spatially continuous RF contours, thresholds for Gabor-sampled contours show a characteristic improvement between RF2 and RF4, and thresholds for randomized phases (open circles) are slightly although reliably more elevated than those for Gabor in cosine phase (filled circles). However, in both conditions,

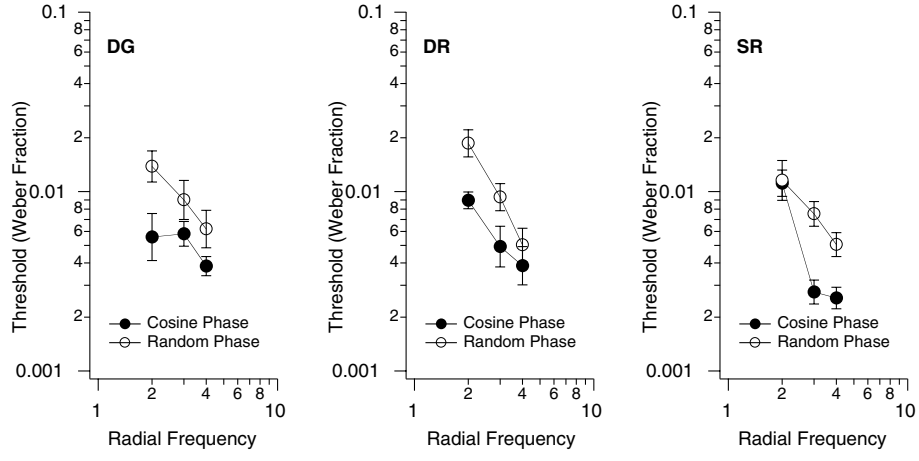

Fig. 2. Detecting spatial-RFs. Each graph shows spatial-RF amplitude thresholds plotted vs. radial frequency for one of three observers. Cosine-phase and random-phase conditions are represented by filled and open symbols respectively. Thresholds are reported as proportions of mean test radius (i.e. Weber fractions). Error bars show 95% confidence intervals (±2 SD).

thresholds for Gabor-sampled RFs fall within the range of those measured for continuous RF contours. Such low thresholds cannot be explained by local curvature detection (Loffler et al., 2003; Wilkinson et al., 1998) and therefore suggest that, as in the case of continuous contours, modulation detection in Gabor-sampled spatial-RF patterns is mediated by mechanisms that encode global RF structure.

4. Detecting motion-RFs

Most observers viewing a motion-RF pattern (e.g. panels D through F in Fig. 1) report a vivid percept of form. In the present section, we report the results from three experiments designed to test observer sensitivity to the global structure of motion-RF contours.

In a first experiment, observers discriminated between a coherent motion-RF and an incoherent version in which speeds were randomly permuted across elements; this random permutation produces identical local motions in both intervals but destroys the structure of the RF modulation in the null interval. Thresholds were obtained by varying the overall motion amplitude of the display.

Fig. 3 plots the motion-RF detection thresholds of three observers as a function of radial frequency. While absolute thresholds between spatial-RFs and motion-RFs cannot be compared directly because they lie on different scales, it is possible to compare the magnitude of the effect of radial frequency on the detection of RF modulation in the spatial and motion domains. Results show that, unlike for spatial-RFs, detection thresholds for motion-RFs either increase or remain approximately constant over the radial-frequency range of 2–4 cycles.

We conducted a second experiment to measure the ability of observers to integrate motion-RF information over space. The paradigm was similar to the first experiment—observers discriminated between coherent and incoherent motion-RF4 contours—but motion amplitude thresholds were measured for "partial" motion-RF4s in which only an angular section (i.e. a pie wedge) of the RF4 modulation was preserved and the remaining section was made incoherent via random speed permutations between Gabor elements. Varying the polar angle of the coherent section allowed us to manipulate the number of Gabor elements that fell within the coherent section.

Fig. 4 plots the motion-detection thresholds of two observers as a function of the number of Gabor

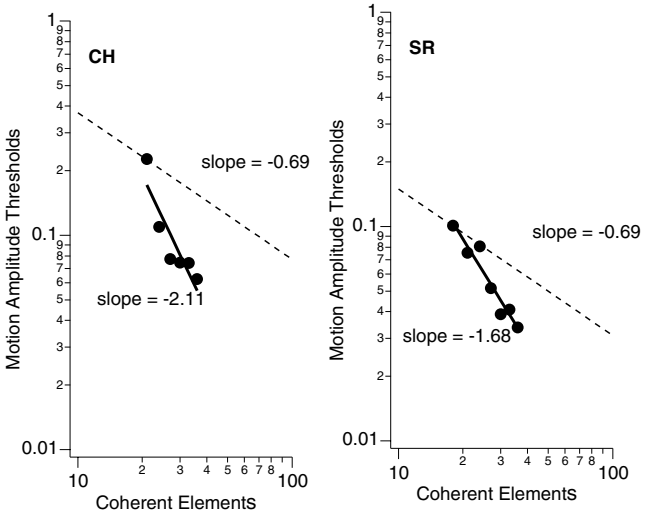

Fig. 4. Spatial-summation over motion-RF4s. Each graph shows motion-RF4 amplitude thresholds vs. the number of Gabor elements within the contour's coherent section. Error-bars have been omitted for clarity but are comparable to those in Fig. 3. Dashed lines show predictions from probability summation.

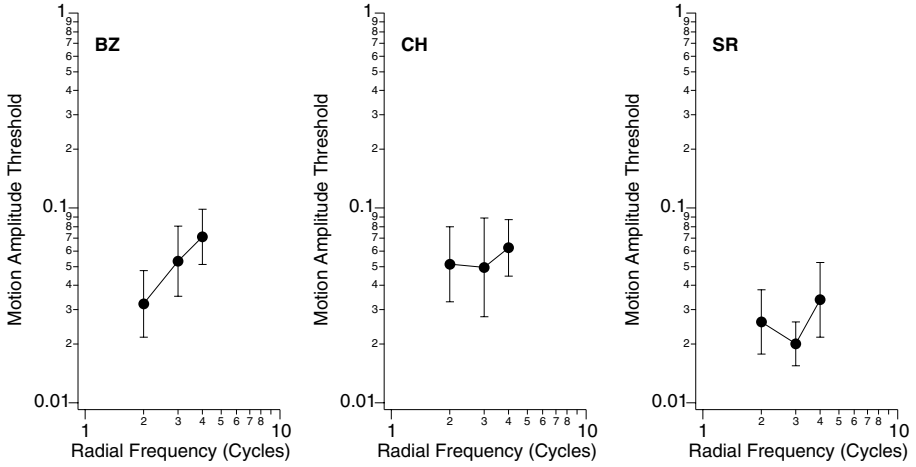

Fig. 3. Detecting motion-RFs. Each graph shows motion-RF amplitude thresholds plotted vs. radial frequency for one of three observers. Error bars show 95% confidence intervals (±SD).

elements in the RF4's coherent section. Dashed lines show threshold improvements assuming local contour information was pooled across elements according to a probability-summation rule. As in a similar study on partial spatial-RFs (Loffler et al., 2003), the slope of the probability-summation curve was estimated by computing the negative of the inverse of the average psychometric slope across observers and conditions in this experiment.

Results show that detection thresholds improve as the coherent section's angle increases and includes more Gabor elements. However, in line with a previous study on partial spatial-RFs (Loffler et al., 2003), thresholds improve at a higher rate than predicted by probability summation—in other words, spatial-summation thresholds are lower than those expected from the statistical recruitment of independent mechanisms that encode local contour properties such as speed differences between neighbouring elements. These results therefore provide direct evidence that motion-RFs are processed by mechanisms sensitive to global structure.

Also noteworthy is our finding that spatial-summation curves for motion-RFs have steeper slopes than those previously reported for spatial-RFs: whereas the two observers in the present study exhibit summation slopes of −2.11 and −1.68 respectively, slopes measured for spatial-RFs never exceed linear summation, or −1.0 (Loffler et al., 2003). Interestingly, the spatial-summation slopes reported herein are also steeper than those for measured for the detection of biological motion and rival those for discriminating biological motion (Neri, Morrone, & Burr, 1998). As we further argue in Section 7, the steep slopes we have measured for motion-RFs constitute a strong piece of evidence that motion- and spatial-RFs are encoded by separate neural pathways.

Finally, in a third experiment, we determined whether observers can discriminate between motion-RFs of different radial frequencies with motion amplitudes of 0.5. Three observers (AC, MK, and SR) participated in a "match-to-sample" task in which observers were asked to match the perceived structure of a motion-RF test to the global structure of one of four possible *spatial*-RFs (RF1, RF2, RF3, or RF4). Note that the radial phase of motion RFs was randomized over trials such that observers could not base their judgment on local motion cues.

Results from this experiment do not require plotting as all observers easily achieved a performance of 100% for all motion-RFs involved. We also repeated the experiment with gratings that were windowed by hard-edge rather than Gaussian apertures and found identical results. Data from this third experiment confirm casual reports that observers can readily abstract global structure from motion-RFs irrespective of the phase of the RF modulation.

5. Experiment 3: detecting spatial-RF tests on motion-RF pedestals

In this section, we investigate how a *motion*-RF4 pedestal influences the detection of a superimposed *spatial*-RF4 test. Thresholds were measured for tests whose radial modulation was either in-phase (panel G of Fig. 1) or in anti-phase (panel H of Fig. 1) with respect to the pedestal. Although test and pedestal were always in one of two relative phases (0° or 180°), the absolute phase of the combined stimulus was randomized on each trial. Thresholds were also measured over a large range of pedestal motion amplitudes that extended from virtually static up to the quarter-cycle limit (i.e. a motion amplitude of 1.0).

Fig. 5A shows detection thresholds for the spatial-RF4 test as a function of motion-RF4 pedestal amplitude. As would be expected, detection thresholds at low pedestal amplitudes are near the baseline (dashed line) obtained with spatial-RF4s tests presented in isolation (see Experiment 1). However, as pedestal amplitude increased, detection thresholds increased although at a shallower rate for in-phase than anti-phase pedestals. For high-amplitude anti-phase pedestals, detection thresholds reached nearly a 10-fold elevation.

Individual psychometric functions obtained at relatively high pedestal amplitudes yield additional clues as to how motion-RF pedestals influence the detection of spatial-RF tests. Fig. 5B compares the psychometric function (i.e. proportion correct vs. amplitude of the spatial-RF test) for in-phase and anti-phase pedestals with 0.5 motion amplitude. Data reveal that, for in-phase pedestals, performance gradually improves from chance to near-perfect levels as test amplitude is increased. For anti-phase pedestals, however, performance falls significantly *below* chance at low test amplitudes before rising back to chance at moderate test amplitudes and finally rising above chance at higher test amplitudes. Note that test amplitudes leading to near-perfect performance for the in-phase mask conditions produce only chance performance for anti-phase pedestals, and that significantly higher test amplitudes are required to overcome the effects of anti-phase motion pedestals.

If observers could segregate the spatial-RF test and the motion-RF pedestal into two separate perceptual entities, then masking would presumably not occur. This clearly is not the case, as the present experiment demonstrates that high-amplitude motion pedestals dramatically interefere with mechanisms mediating spatial-RF detection. The below-chance regime in psychometric functions for anti-phase pedestals further suggests that motion-RFs and spatial RFs ultimately share a common (or cue-invariant) representation at some stage in the visual system since observers are manifestly incapable of perceptually segregating spatial-RFs from superimposed motion-RFs.

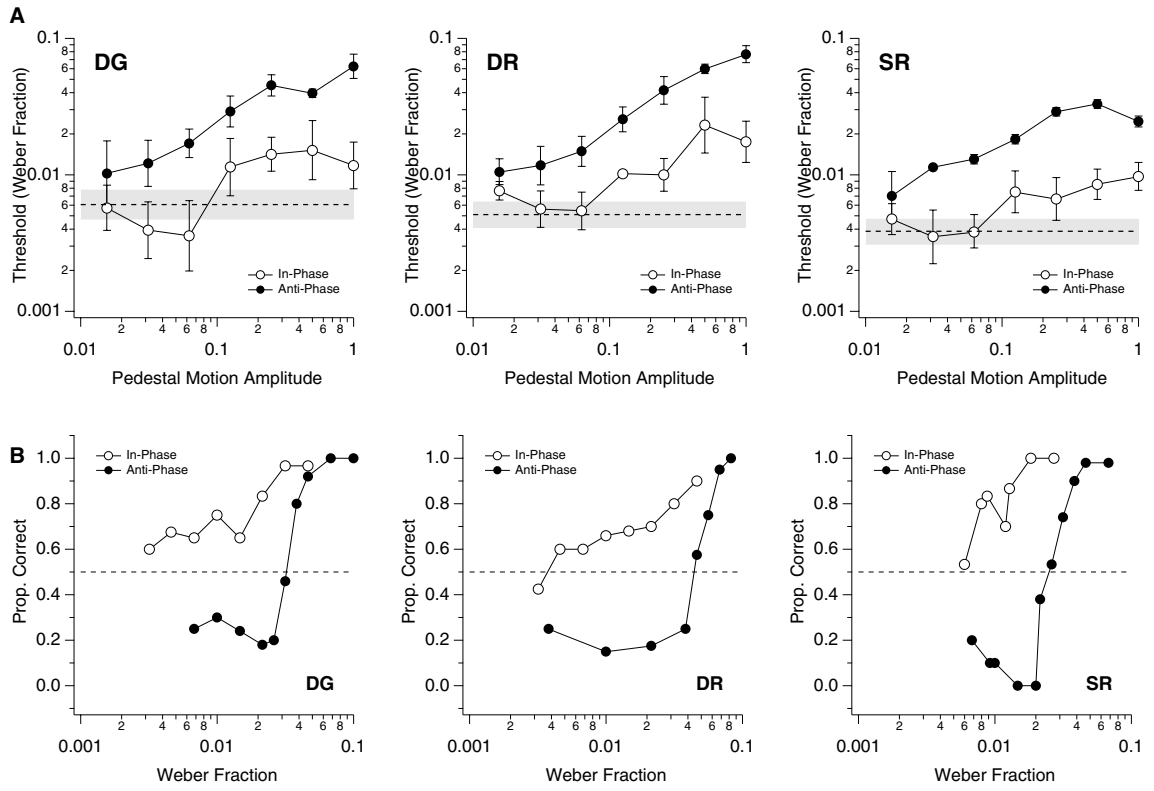

Fig. 5. Results for detecting spatial-RF4 tests superimposed on motion-RF4 pedestals. (A) Detection thresholds of three observers for spatial-RF4 tests are plotted as a function of motion-RF4 pedestal amplitude. Test and pedestal are either in-phase (open circles) or in anti-phase (solid circles). Error bars show 95% confidence intervals for pedestal data (±2 SD). Dashed lines show baseline detection thresholds for spatial-RF4 (see Fig. 1) and gray-shaded area shows baseline confidence intervals (±2 SD). (B) Psychometric functions plotting proportion correct vs. amplitude of the spatial-RF test for detecting spatial-RF4s on motion-RF4s pedestals with amplitudes of 0.5. Dashed lines show chance performance (50%) for a two-alternative forced-choice task.

A key question, then, is at what level in the visual hierarchy is this cue-invariant representation of RF structure implemented? The present experiment yields one potential clue in this respect: although the threshold vs. pedestal amplitude curves shown in Fig. 5A show some hints of subthreshold facilitation—or "dipper" function (Legge & Foley, 1980; Nachmias & Sansbury, 1974)—the substantial overlap in confidence intervals between no-pedestal and pedestal data suggests little or no perceptual interaction between motion- and spatial-RFs near threshold levels. In previous studies, however, our laboratory has shown clear dipper functions for detecting *spatial*-RF tests superimposed on *spatial*-RF pedestals, although the amount of facilitation varies with radial frequency (Wilkinson, Loffler, Wilson, & King, 2002). The lack of significant subthreshold summation between spatial-RFs and motion-RFs reported here is therefore consistent with the notion that spatial-form and motion-form are encoded by different pathways through early stages of vision and that the cue-invariant representation these pathway ultimately share is achieved at later stages in the visual hierarchy. Data from the following section further support this interpretation.

6. Experiment 4: other motion pedestals

In a series of conditions, we tested whether threshold elevations measured for spatial-RF4 tests in the presence of motion-RF4 pedestals are attributable simply to the presence of motion per se or whether spatial-form mechanisms are selective for the structure of motion pedestals. As in the previous experiment, observers were instructed to detect a spatial-RF4 test superimposed on various dynamic pedestals consisting either of flicker (Fig. 1I), pure contraction (Fig. 1J), pure expansion (Fig. 1K), or randomly permuted speeds (Fig. 1L). Flicker pedestals were composed of the linear sum of in-phase and anti-phase motion-RF4 pedestals with identical amplitudes; the resulting pedestal preserves all the local temporal properties of the stimulus but creates a percept of flicker (i.e. counterphasing) rather than of directional motion. Contraction and expansion were obtained from motion-RF0 pedestals with negative or positive motion amplitudes respectively. Randomized pedestals were identical to the motion-RF4 patterns used in Experiment 2 where global structure was destroyed but local motion statistics were preserved by randomly permuting speeds across Gabor elements.

Thresholds were measured only for a single pedestal amplitude of 0.5 for all the conditions described in this section.

Fig. 6 shows detection thresholds of three observers for spatial-RF4 tests embedded in various types of dynamic pedestals. Results show a similar pattern across observers. As reported in the previous experiment, detection thresholds for a spatial-RF4 tests are significantly more elevated in the presence of in-phase and anti-phase motion-RF4 pedestals. However, flicker, contraction, expansion, and randomized pedestals had no significant effect on thresholds with the exception of a slight but significant threshold elevation in the randomized mask condition for one observer.

The finding that flickering RF4 pedestals do not interfere with the detection of a spatial-RF4 test confirms that motion, rather than temporal energy alone, is responsible for interferring with the perception of spatial-form because flicker and motion pedestals have identical local and global spatiotemporal properties and differ only in their directional vs. non-directional characteristics. The presence of a motion-RF0 pedestal (either expanding or contracting) has no measurable effect on thresholds, and this indicates that threshold elevations caused by motion pedestals are selective for similarities in the global structure of spatial tests and motion pedestals.

The finding that randomized motion pedestals have little or no effect on the detection of spatial-RF tests is particularly interesting given that they do not agree with a previous study where spatial path integration is disrupted by elements whose motion introduce perceived positional jitter away from the path's backbone (Hayes, 2000). If, as claimed by the author, local motion cues can masquarade as spatial cues in spatial-form perception, we would expect significant threshold elevations in the random-pedestal condition as even very small amounts of positional jitter are known to significantly affect the ability to integrate spatial-RFs (Loffler et al., 2003). Because all the pedestal conditions reported in this section have identical local motion statistics (except the flicker pedestal which is non-directional), one would expect for the effects of speed to have similar effect on detection thresholds for the spatial-RF4 test. As results in Fig. 6 clearly show, however, motion pedestals produce widely different results in terms of threshold elevation and therefore strongly suggest that the *global* motion structure of the pedestal is the key variable.

7. Discussion

7.1. Local vs. global interference of motion cues on spatial-form perception

Results from this study show that observers can encode the global structure of spatial-RF (Experiment 1) and motion-RF (Experiment 2) contours. But are the two types of stimuli encoded by the same visual mechanisms? And if not, at what level in the visual hierarchy does motion interfere with the coding of spatial-form? One possibility is that stimuli from Experiments 1 and 2 are analyzed by distinct pathways that encode global RF structure separately in the spatial and motion domain. Under this "global interference" scenario, threshold elevations observed in the in-phase/anti-phase pedestals conditions (Experiment 3) would reflect interference between mechanisms encoding motion-form and spatial-form at a relatively high level in the visual hierarchy.

Another possibility, however, is that threshold elevations by in-phase/anti-phase motion pedestals reflect a low-level influence of local motion cues onto local spatial cues. Because the drifting carrier of a Gabor element can introduce a perceived shift in the spatial position of the envelope (De Valois & De Valois, 1991), it is possible that spatial-form and motion-form are both encoded by

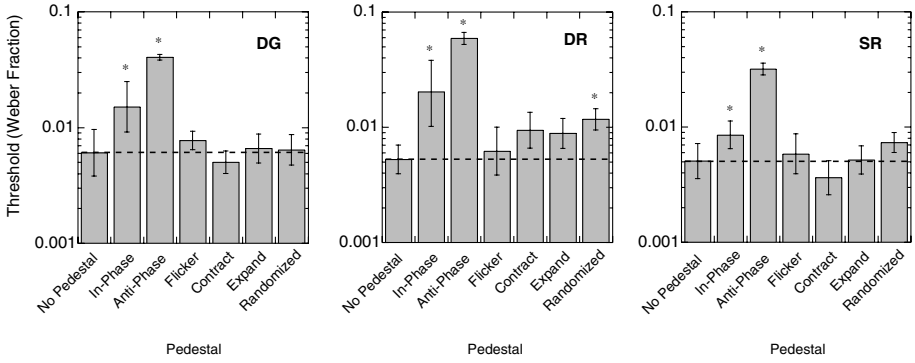

Fig. 6. Results for detecting a spatial-RF4 test superimposed on a variety of motion pedestals. Detection thresholds of three observers are shown for spatial-RF4 tests superimposed on flickering, contracting, expanding, and randomized pedestals of fixed amplitude (0.5). Detection thresholds for spatial RF4s in isolation (dashed line and no-pedestal condition), in-phase, and anti-phase motion-RF4 masks are also included for comparison. Error bars report 95% confidence intervals. Statistically significant deviations from baseline (two-tail Student t-test, df $= 6$, $p < 0.01$) are indicated by a star symbol.

spatial-form mechanisms—that is, under this "local interference" scenario, motion cues would effectively supply positional cues to spatial-form pathways and motion-form pathways would not contribute to perception. In the following paragraphs, we systematically review evidence collected in this study and conclude that our results reflect a high-level interference between mechanisms encoding spatial-form and motion-form.

A first cue that favors the "global interference" scenario is obtained by comparing detection thresholds for spatial- and motion-RFs. Results show that thresholds for motion-RFs either tend to increase or stay relatively constant over the range of 2–4 cycles (Fig. 3) whereas thresholds for spatial-RFs decrease substantially over the same range (Fig. 2). This discrepancy suggests that the perception of spatial-RFs and motion-RFs is mediated by different neural processes.

The second and perhaps most diagnostic test for local vs. global interference scenarios comes from the spatial-summation data on motion-RFs in Experiment 2. The summation slope of less than −1.0 reported for *spatial*-RFs by a previous study (Loffler et al., 2003) suggests neural mechanisms that recruit local contour detectors more efficiently than probability summation but integrate local contour information less efficiently than matched linear filtering. By comparison, our results for *motion*-RFs show summation slopes considerably in excess of −1.0 and therefore imply a qualitatively different integration scheme. Indeed, a summation slope steeper than −1.0 constitutes evidence for mechanisms that combine local information in a synergistic (i.e. nonlinear) fashion across space. For instance, a plausible neural implementation of synergistic summation for motion-RFs may consist of local motion detectors that mutually reinforce each other through positive feedback. The discrepancy between summation slopes for spatial- and motion-RFs—and the qualitatively different spatial-summation schemes they imply—therefore provides strong evidence that the two types of stimuli are initially processed by separate neural pathways. This conclusion is further supported by the observation that summation slopes steeper than −1.0 have been reported for other complex motion patterns such as biological motion (Neri et al., 1998) but are otherwise uncommon in vision research.

The use of hard-edge apertures for the motion-RFs in Experiment 2 adds further evidence to the notion that a low-level interference of motion cues on spatial cues (i.e. the "local interference" scenario) is not involved in the perception of global structure in motion-RFs. Indeed, the perceived positional shift induced by a grating drifting behind a Gaussian aperture is significantly reduced if the Gaussian aperture is replaced by a hard-edge one (Zhang, Yeh, & De Valois, 1993). Our finding that hard-edge apertures do not impair the perception of global structure in motion-RFs therefore strongly suggests that motion-form, not illusory spatial shifts in local position, is the relevant variable.

In Experiment 3, motion-RF4 pedestals produced little evidence of a facilitation regime at low pedestal amplitudes. As we argued in Experiment 3, the lack of subthreshold facilitation between spatial-RFs and motion-RFs is consistent with the idea that spatial-form and motion-form are initially encoded by different pathways and that the cue-invariant representation these pathway ultimately share is achieved at a later stage in the visual hierarchy.

Results from Experiment 4 provide additional evidence that masking effects observed in Experiment 3 are mediated by a high-level interference between mechanisms encoding spatial-form and motion-form. Whereas in-phase and anti-phase RF4 pedestals in Experiment 3 resulted in significant threshold elevation (in some cases a 10-fold increase), other conditions such as expansion, contraction, or randomized pedestals produced little or no measurable effect. According to the local hypothesis, motion pedestals with identical amplitudes should all produce significant threshold elevations since it has previously been shown that even small amounts of positional jitter increase detection threshold for spatial-RFs significantly (Loffler et al., 2003). In this respect, our finding that randomized motion pedestals have virtually no effect is particularly difficult to explain with the "local interference" scenario.

Overall, results from the present study strongly favor the high-level "global interference" scenario where mechanisms mediating motion-form perception interfere with mechanisms encoding spatial-form. However, this conclusion raises the puzzling question of why we have failed to observe the effect of "local interference" that has been reported in a previous study on path detection with drifting Gabors (Hayes, 2000). The answer to this question may lie partly in the fact that path integration, by definition, is a spatial-form *detection* task where observers operate under a regime in which spatial-form is either absent or barely visible. By comparison, our study can be understood in terms of a spatial-form *discrimination* task that operates under a regime where spatial-form is always highly salient and observers discriminate between circles and slight deviations from circularity.

Physiological evidence suggests a functional separation between the analysis of spatial cues and motion cues, but one that also allows for communication between those two pathways at all levels of the visual hierarchy. Such a scheme where cross-pathway interactions exist at multiple levels could potentially explain why the present study has failed to observe the "local interference" effects reported in previous studies. For instance, in a spatial-form *detection* regime where global structure is either absent or barely visible (e.g. spatial path integration), the "local interference" scenario may

dominate, perhaps in an attempt by the visual system to combine local spatial and motion cues under high-noise conditions to improve the detection of global structure of any kind. However, in a spatial-form *discrimination* regime where spatial-form is highly visible, spatial-form and motion-form pathways may compete for a unique representation of global structure. Under this ''global interference'' scenario, higher-level stages concerned with global structure may ignore (perhaps via feedback suppression) low-level cues that do not contribute—or are inconsistent with—spatial-form or motion-form. A multi-level scheme such as this one could account for the selective masking effects we have measured with various types of motion pedestals: for instance, according to this line of thought, an anti-phase motion-RF pedestal may compete for a unique representation of global structure with a spatial-RF test, whereas a randomized motion pedestal may be ignored because it lacks any global structure.

Similar ideas have been proposed for cue-specific integration in spatial and motion pathways (Hupe et al., 1998; Lamme & Roelfsema, 2000; Li, Thier, & Wehrhahn, 2000; Lorenceau & Alais, 2001; Lorenceau & Zago, 1999; Salin & Bullier, 1995; Sugase, Yamane, Ueno, & Kawano, 1999; Tolias, Smirnakis, Augath, Trinath, & Logothetis, 2001; Zipser, Lamme, & Schiller, 1996). Given the ubiquitous presence of feedback connections in the visual system, it may be possible to capitalize on the time delays intrinsic to feedback in order to gain additional psychophysical insight into the mechanisms that mediate interactions between mechanisms encoding spatial-form and motion-form.

7.2. Physiological correlates

Influential theories on mammalian vision propose that spatial cues and motion cues in the retinal image are processed separately by distinct functional streams commonly labeled as the ventral and dorsal pathways respectively (Baizer, Ungerleider, & Desimone, 1991; DeYoe & Van Essen, 1988; Goodale & Milner, 1992; Merigan & Maunsell, 1993; Shipp, 1995; Ungerleider & Desimone, 1982; Van Essen & Maunsell, 1983; Zeki & Shipp, 1988). As the ventral pathway proceeds from primary visual cortex along inferior temporal cortex, local spatial cues—such as position, orientation, and scale—are combined into representations of form that range from simple objects such as closed contours (Wilkinson et al., 2000) to more complex objects such as human faces (Allison, Puce, Spencer, & McCarthy, 1999; Kanwisher, McDermott, & Chun, 1997). Similarly, the dorsal pathway projects from primary visual cortex to areas of posterior parietal cortex sensitive to global patterns of motion that include optic flow (Duffy & Wurtz, 1997; Graziano, Andersen, & Snowden, 1994) and biological motion (Vaina, Solomon, Chowdhury, Sinha, & Belliveau, 2001). Results from these studies are consistent with a parallel-streams architecture whereby global visual analysis takes place along independent cue-specific pathways (Braddick, O'Brien, Wattam-Bell, Atkinson, & Turner, 2000; Livingstone & Hubel, 1988).

In contrast to cue specificity, the notion of cue invariance proposes that neural mechanisms involved in computing global spatial structure and global motion structure do not distinguish between cue types. Anatomical evidence of reciprocal ventro-dorsal connections over most of the visual system's hierarchy argues against a complete functional segregation and supports the view that ventral and dorsal pathways interact (Felleman & Van Essen, 1991; Maunsell & van Essen, 1983; Merigan & Maunsell, 1993; Sawatari & Callaway, 1996; Ungerleider & Desimone, 1986; Young, 1992). Several studies show that dorsal areas respond to motion defined by cues such as luminance, texture, and color (Albright, 1992; Geesaman & Andersen, 1996; Stoner & Albright, 1992) and that ventral areas are sensitive to global shapes defined purely by coherent motion (Sary, Vogels, & Orban, 1993; Wang et al., 1999). Reports that cue invariance can arise in visual areas as low as V1 and V2 (Gegenfurtner, Kiper, & Fenstemaker, 1996; Grill-Spector, Kushnir, Edelman, Itzchak, & Malach, 1998; Leventhal, Wang, Schmolesky, & Zhou, 1998) are consistent with an architecture that facilitates cross-talk between cue-specific pathways throughout the visual system's functional hierarchy.

Far from being mutually exclusive, cue specificity and cue invariance may play complementary functional roles: indeed, ventral and dorsal pathways may specialize in answering different questions about a visual scene (e.g. what and where) without necessarily monitoring which types of visual cues are involved. The new class of stimuli we have introduced in this present paper, with its particular ability to physically superimpose spatial-form and motion-form, is amenable to a variety of behavioral and physiological techniques and offers a powerful paradigm to understand cue-specific and cue-invariant representations in the human visual system.

Acknowledgements

We thank anonymous reviewers for their suggestions and Gunter Loeffler for useful discussions on this work. This work has been supported by grant OP227224 from the Natural Science and Engineering Council of Canada.

Appendix A. Additional stimulus specifications

Spatial-RFs were sampled by an array of Gabor elements that were distributed in equal polar-angle

intervals. The angle α of the ith element with respect to the stimulus center is given by

$$\alpha_i = \frac{2\pi n_i}{N}, \quad n = 0, 1, \ldots, N-1 \tag{A.1}$$

where N represents the total number of Gabors. The distance R from the ith element to the stimulus' center is given by

$$R_i = R_{\text{mean}}[1 + A_s \cos(\omega_s \alpha_i + \beta_s)] \tag{A.2}$$

where A_s and ω_s correspond to the modulation amplitude and radial frequency of the *spatial* contour, and β_s represents the contour's phase offset with respect to the sampling grid. The phase β_s was quantized to the same values of polar angle α_i to ensure that sinusoidal modulations were sampled at the same points regardless of how the pattern was rotated in the xy plane.

Once Gabors were properly positioned, the spatiotemporal profile g of the ith element was defined as the product of a Gaussian envelope and a drifting sinusoidal carrier given by

$$g_i(x, y, t) = \exp\left[-\frac{(R - R_i)^2}{2\sigma^2}\right] \cdot \cos\left[2\pi((x - x_i)\cos\theta_i - (y - y_i)\sin\theta_i) + \phi_i(t)\right] \tag{A.3}$$

where x_i and y_i are the element's Cartesian center coordinates, σ is the space constant of the circular Gaussian envelope, θ is the orientation of the spatial carrier, and ϕ is a time-varying function that controls the phase of the element's carrier. The collinearity of the RF contour was obtained by aligning each element's orientation with the contour's local tangent.

For the motion RFs, the time-varying function ϕ specified the carrier phase of the ith element on the jth movie frame q as

$$\phi_{i,j} = A_m \cos(\omega_m \alpha_i + \beta_m) \cdot q_j \pi/2 + \Delta_i, \quad q = 0, 1, \ldots, Q-1 \tag{A.4}$$

where A_m defines the overall speed (or "motion amplitude") of the display, β_m determines the motion RF's phase (or, equivalently, it's orientation in the xy plane) and Q denotes the total number of frames. A_m can be no greater than 1.0 in order to respect the quarter-cycle limit on the $q_j\pi/2$ term which, at a maximum motion amplitude of 1.0, advances carrier phase by 90° between successive frames. The term $\cos(\omega_m \alpha_i + \beta_m)$ evaluates to a constant for each element and plays a similar role as in spatial RF contours, namely to impose a sinusoidal modulation as a function of polar angle. Lastly, Δ_i is a random offset that specifies the initial spatial phase of the ith element's carrier.

References

Alais, D., van der Smagt, M. J., van den Berg, A. V., & van de Grind, W. A. (1998). Local and global factors affecting the coherent motion of gratings presented in multiple apertures. *Vision Research, 38*(11), 1581–1591.

Albright, T. D. (1992). Form-cue invariant motion processing in primate visual cortex. *Science, 255*(5048), 1141–1143.

Allison, T., Puce, A., Spencer, D. D., & McCarthy, G. (1999). Electrophysiological studies of human face perception. I. Potentials generated in occipitotemporal cortex by face and non-face stimuli. *Cerebral Cortex, 9*(5), 415–430.

Anderson, S. J., & Burr, D. C. (1987). Receptive field size of human motion detection units. *Vision Research, 27*(4), 621–635.

Baizer, J. S., Ungerleider, L. G., & Desimone, R. (1991). Organization of visual inputs to the inferior temporal and posterior parietal cortex in macaques. *Journal of Neuroscience, 11*(1), 168–190.

Bex, P. J., & Dakin, S. C. (2002). Comparison of the spatial-frequency selectivity of local and global motion detectors. *Journal of the Optical Society of America, A, Optics, Image Science, and Vision, 19*(4), 670–677.

Bex, P. J., Simmers, A. J., & Dakin, S. C. (2001). Snakes and ladders: The role of temporal modulation in visual contour integration. *Vision Research, 41*(27), 3775–3782.

Blakemore, C., & Campbell, F. W. (1969). On the existence of neurones in the human vision system selectively sensitive to the orientation and size of retinal images. *Journal of Physiology, 203*, 237–260.

Braddick, O. J., O'Brien, J. M., Wattam-Bell, J., Atkinson, J., & Turner, R. (2000). Form and motion coherence activate independent, but not dorsal/ventral segregated, networks in the human brain. *Current Biology, 10*(12), 731–734.

Brainard, D. H. (1997). The Psychophysics Toolbox. *Spatial Vision, 10*, 443–446.

Campbell, F. W., & Robson, J. G. (1968). Application of Fourier analysis to the visibility of gratings. *Journal of Physiology, 197*, 551–566.

Croner, L. J., & Albright, T. D. (1997). Image segmentation enhances discrimination of motion in visual noise. *Vision Research, 37*(11), 1415–1427.

De Valois, R. L., & De Valois, K. K. (1991). Vernier acuity with stationary moving Gabors. *Vision Research, 31*(9), 1619–1626.

De Valois, K. K., & Tootell, R. B. (1983). Spatial-frequency-specific inhibition in cat striate cortex cells. *Journal of Physiology, 336*, 359–376.

DeAngelis, G. C., Freeman, R. D., & Ohzawa, I. (1994). Length and width tuning of neurons in the cat's primary visual cortex. *Journal of Neurophysiology, 71*(1), 347–374.

DeYoe, E. A., & Van Essen, D. C. (1988). Concurrent processing streams in monkey visual cortex. *Trends in Neurosciences, 11*(5), 219–226.

Duffy, C. J., & Wurtz, R. H. (1997). Planar directional contributions to optic flow responses in MST neurons. *Journal of Neurophysiology, 77*(2), 782–796.

Efron, B., & Tibshirani, R. J. (1993). *An introduction to the bootstrap*. New York: Chapman & Hall.

Felleman, D. J., & Van Essen, D. C. (1991). Distributed hierarchical processing in the primate cerebral cortex. *Cerebral Cortex, 1*(1), 1–47.

Field, D. J., Hayes, A., & Hess, R. F. (1993). Contour integration by the human visual system: Evidence for a local "association field". *Vision Research, 33*(2), 173–193.

Fredericksen, R. E., & Hess, R. F. (1997). Temporal detection in human vision: Dependence on stimulus energy. *Journal of the Optical Society of America A Optics & Image Science, 14*(10), 2557–2569.

Geesaman, B. J., & Andersen, R. A. (1996). The analysis of complex motion patterns by form/cue invariant MSTd neurons. *Journal of Neuroscience, 16*(15), 4716–4732.

Gegenfurtner, K. R., Kiper, D. C., & Fenstemaker, S. B. (1996). Processing of color, form, and motion in macaque area V2. *Visual Neuroscience, 13*(1), 161–172.

Geisler, W. S. (1999). Motion streaks provide a spatial code for motion direction. *Nature, 400*(6739), 65–69.

Goodale, M. A., & Milner, A. D. (1992). Separate visual pathways for perception and action. *Trends in Neurosciences, 15*(1), 20–25.

Graziano, M. S., Andersen, R. A., & Snowden, R. J. (1994). Tuning of MST neurons to spiral motions. *Journal of Neuroscience, 14*(1), 54–67.

Grill-Spector, K., Kushnir, T., Edelman, S., Itzchak, Y., & Malach, R. (1998). Cueinvariant activation in object-related areas of the human occipital lobe. *Neuron, 21*(1), 191–202.

Hayes, A. (2000). Apparent position governs contour-element binding by the visual system. *Proceedings of the Royal Society of London Series B: Biological Sciences, 267*(1450), 1341–1345.

Hess, R. F., & Dakin, S. C. (1997). Absence of contour linking in peripheral vision. *Nature, 390*(6660), 602–604.

Hubel, D. H., & Wiesel, T. N. (1968). Receptive fields and functional architecture of monkey striate cortex. *Journal of Physiology, 195*, 215–243.

Hupe, J. M., James, A. C., Payne, B. R., Lomber, S. G., Girard, P., & Bullier, J. (1998). Cortical feedback improves discrimination between figure and background by V1, V2 and V3 neurons. *Nature, 394*(6695), 784–787.

Kanwisher, N., McDermott, J., & Chun, M. M. (1997). The fusiform face area: A module in human extrastriate cortex specialized for face perception. *Journal of Neuroscience, 17*(11), 4302–4311.

Lamme, V. A., & Roelfsema, P. R. (2000). The distinct modes of vision offered by feedforward and recurrent processing. *Trends in Neurosciences, 23*(11), 571–579.

Legge, G. E., & Foley, J. M. (1980). Contrast masking in human vision. *Journal of the Optical Society of America, 70*(12), 1458–1471.

Lehky, S. R. (1985). Temporal properties of visual channels measured by masking. *Journal of the Optical Society of America A—Optics and Image Science, 2*(8), 1260–1272.

Leventhal, A. G., Wang, Y., Schmolesky, M. T., & Zhou, Y. (1998). Neural correlates of boundary perception. *Visual Neuroscience, 15*(6), 1107–1118.

Li, H. C., & Kingdom, F. A. (1999). Feature specific segmentation in perceived structure-from-motion. *Vision Research, 39*(5), 881–886.

Li, H. C., & Kingdom, F. A. (2001). Motion-surface labeling by orientation, spatial frequency and luminance polarity in 3-D structure-from-motion. *Vision Research, 41*(28), 3873–3882.

Li, W., Thier, P., & Wehrhahn, C. (2000). Contextual influence on orientation discrimination of humans and responses of neurons in V1 of alert monkeys. *Journal of Neurophysiology, 83*(2), 941–954.

Livingstone, M. S., & Hubel, D. H. (1988). Segregation of form, colour, movement and depth: Anatomy, physiology, and perception. *Science, 240*, 740–749.

Loffler, G., & Wilson, H. R. (2001). Detecting shape deformation of moving patterns. *Vision Research, 41*(8), 991–1006.

Loffler, G., Wilson, H. R., & Wilkinson, F. (2003). Local and global contributions to shape discrimination. *Vision Research, 43*(5), 519–530.

Lorenceau, J. (1996). Motion integration with dot patterns: Effects of motion noise and structural information. *Vision Research, 36*(21), 3415–3427.

Lorenceau, J., & Alais, D. (2001). Form constraints in motion binding. *Nature Neuroscience, 4*(7), 745–751.

Lorenceau, J., & Shiffrar, M. (1992). The influence of terminators on motion integration across space. *Vision Research, 32*(2), 263–273.

Lorenceau, J., & Zago, L. (1999). Cooperative and competitive spatial interactions in motion integration. *Visual Neuroscience, 16*(4), 755–770.

Mandler, M. B., & Makous, W. (1984). A three channel model of temporal frequency perception. *Vision Research, 24*, 1881–1887.

Maunsell, J. H., & van Essen, D. C. (1983). The connections of the middle temporal visual area (MT) and their relationship to a cortical hierarchy in the macaque monkey. *Journal of Neuroscience, 3*(12), 2563–2586.

Merigan, W. H., & Maunsell, J. H. R. (1993). How parallel are the primate visual pathways? *Annual Review of Neuroscience, 16*, 369–402.

Mingolla, E., Todd, J. T., & Norman, J. F. (1992). The perception of globally coherent motion. *Vision Research, 32*(6), 1015–1031.

Morrone, M. C., Burr, D. C., & Vaina, L. M. (1995). Two stages of visual processing for radial and circular motion. *Nature, 376*(6540), 507–509.

Nachmias, J., & Sansbury, R. V. (1974). Letter: Grating contrast: Discrimination may be better than detection. *Vision Research, 14*(10), 1039–1042.

Neri, P., Morrone, M. C., & Burr, D. C. (1998). Seeing biological motion. *Nature, 395*(6705), 894–896.

Pelli, D. G. (1997). The VideoToolbox software for visual psychophysics: Transforming numbers into movies. *Spatial Vision, 10*, 437–442.

Pinter, R. B., & Harris, L. R. (1981). Temporal and spatial response characteristics of the cat superior colliculus. *Brain Research, 207*(1), 73–94.

Ross, J., Badcock, D. R., & Hayes, A. (2000). Coherent global motion in the absence of coherent velocity signals. *Current Biology, 10*(11), 679–682.

Salin, P. A., & Bullier, J. (1995). Corticocortical connections in the visual system: Structure and function. *Physiological Reviews, 75*(1), 107–154.

Sary, G., Vogels, R., & Orban, G. A. (1993). Cue-invariant shape selectivity of macaque inferior temporal neurons. *Science, 260*(5110), 995–997.

Sawatari, A., & Callaway, E. M. (1996). Convergence of magno- and parvocellular pathways in layer 4B of macaque primary visual cortex. *Nature, 380*(6573), 442–446.

Shipp, S. (1995). Visual processing. The odd couple. *Current Biology, 5*(2), 116–119.

Stoner, G. R., & Albright, T. D. (1992). Motion coherency rules are form-cue invariant. *Vision Research, 32*(3), 465–475.

Sugase, Y., Yamane, S., Ueno, S., & Kawano, K. (1999). Global and fine information coded by single neurons in the temporal visual cortex. *Nature, 400*(6747), 869–873.

Tolias, A. S., Smirnakis, S. M., Augath, M. A., Trinath, T., & Logothetis, N. K. (2001). Motion processing in the macaque: Revisited with functional magnetic resonance imaging. *Journal of Neuroscience, 21*(21), 8594–8601.

Ungerleider, L. G., & Desimone, R. (1982). Two cortical visual systems. In D. J. Ingle, M. A. Goodale, & R. J. W. Mansfield (Eds.), *Analysis of visual behavior* (pp. 549–580). Cambridge, Massachussets: MIT Press.

Ungerleider, L. G., & Desimone, R. (1986). Cortical connections of visual area MT in the macaque. *Journal of Comparative Neurology, 248*(2), 190–222.

Vaina, L. M., Solomon, J., Chowdhury, S., Sinha, P., & Belliveau, J. W. (2001). Functional neuroanatomy of biological motion perception in humans. *Proceedings of the National Academy of Sciences of the United States of America, 98*(20), 11656–11661.

Van Essen, D. C., & Maunsell, J. H. (1983). Hierarchical organization and functional streams in the visual cortex. *Trends in Neurosciences, 6*, 370–375.

Verghese, P., & Stone, L. S. (1995). Combining speed information across space. *Vision Research, 35*(20), 2811–2823.

Wang, J., Zhou, T., Qiu, M., Du, A., Cai, K., Wang, Z., Zhou, C., Meng, M., Zhuo, Y., Fan, S., & Chen, L. (1999). Relationship between ventral stream for object vision and dorsal stream for spatial vision: An fMRI + ERP study. *Human Brain Mapping, 8*(4), 170–181.

Wilkinson, F., James, T. W., Wilson, H. R., Gati, J. S., Menon, R. S., & Goodale, M. A. (2000). An fMRI study of the selective activation of human extrastriate form vision areas by radial and concentric gratings. *Current Biology, 10*(22), 1455–1458.

Wilkinson, F., Loffler, G., Wilson, H. R., & King, M. (2002). Radial frequency masking and the analysis of complex shape. *Perception, 31*(Suppl), 92.

Wilkinson, F., Wilson, H. R., & Habak, C. (1998). Detection and recognition of radial frequency patterns. *Vision Research, 38*(22), 3555–3568.

Wilson, H. (1999). Non-Fourier cortical processes in texture, form, and motion perception. *Cerebral Cortex, 13*, 445–477.

Wilson, H. R., Ferrera, V. P., & Yo, C. (1992). A psychophysically motivated model for two-dimensional motion perception. *Visual Neuroscience, 9*(1), 79–97.

Young, M. P. (1992). Objective analysis of the topological organization of the primate cortical visual system. *Nature, 358*(6382), 152–155.

Zeki, S., & Shipp, S. (1988). The functional logic of cortical connections. *Nature, 335*(6188), 311–317.

Zhang, J., Yeh, S. L., & De Valois, K. K. (1993). Motion contrast and motion integration. *Vision Research, 33*(18), 2721–2732.

Zipser, K., Lamme, V. A., & Schiller, P. H. (1996). Contextual modulation in primary visual cortex. *Journal of Neuroscience, 16*(22), 7376–7389.